Proc. Natl. Acad. Sci. USA
Vol. 94, pp. 4176–4181, April 1997
Physiology

Sarcoplasmic reticulum Ca^{2+} release flux underlying Ca^{2+} sparks in cardiac muscle

(membranes/ion channels/excitation–contraction coupling)

LOTHAR A. BLATTER*, JÖRG HÜSER*, AND EDUARDO RÍOS†‡

*Department of Physiology, Loyola University Chicago, Maywood, IL 60153; and †Department of Molecular Biophysics and Physiology, Rush University, 1750 West Harrison Street, Chicago, IL 60612

Communicated by Clara Franzini-Armstrong, University of Pennsylvania School of Medicine, Philadelphia, PA, February 14, 1997 (received for review May 15, 1996)

ABSTRACT **Discrete events of Ca^{2+} release from the sarcoplasmic reticulum (SR) have been described in cardiac, skeletal, and smooth muscle. In skeletal muscle these release events originate at individual channels. In cardiac muscle, however, it remains a question of debate whether localized Ca^{2+} release transients, termed Ca^{2+} sparks, originate from single release channels or multiple channels clustered in close vicinity. Generalizing methods used earlier to describe cell-averaged Ca^{2+} release, we derived, as a function of space and time, the flux of Ca^{2+} release that underlies Ca^{2+} sparks. Using the method to analyze spontaneous sparks recorded with confocal microscopy in dissociated cat atrial cells, we obtained in most cases single sparks of Ca^{2+} release that appear to originate from approximately 1-μm-wide regions. In many cases, doublets, triplets, and greater groups of release sparks were observed. This multiplicity, the estimated release flux magnitude, and existing data on the structure of junctions between SR and plasmalemma suggest that individual release sparks result from the opening of multiple Ca^{2+} release channels clustered within discrete SR junctional regions.**

Contraction of cardiac muscle requires release of Ca^{2+} from the sarcoplasmic reticulum (SR) through ryanodine receptors, by Ca^{2+}-induced Ca^{2+} release (1). Since the discovery of local increases in intracellular Ca^{2+} concentration ($[Ca^{2+}]_i$) termed "Ca^{2+} sparks" (2), which occur spontaneously and in response to activation of voltage-gated Ca^{2+} channels (3, 4), a tantalizing prospect can be envisioned: to account for the macroscopic properties of excitation–contraction coupling based on the individual properties of single channels. One necessary step in this program is to decide whether sparks arise from individual channels or the concerted opening of clusters of channels. In favor of the first possibility, Ca^{2+} sparks in cardiac myocytes are of apparently constant amplitude (2); methoxyverapamil reduces the frequency but not the size of sparks elicited by voltage (5), and it is possible to pharmacologically increase the duration of sparks without changing their amplitude (2, 6). On the other hand, recent studies in skeletal muscle revealed elementary events that appear to be much smaller than cardiac sparks, thus suggesting a multichannel origin for the latter (7). Additionally, in cardiac myocytes a smaller, unresolved unit of Ca^{2+} release has been postulated, on the basis of experiments with flash photolysis (8), and a transversal scanning of ventricular myocytes revealed multiplets of sparks occurring almost simultaneously along the transverse tubular membrane (9), indicating that one channel or cluster was activating others, and generally challenging the concept of one channel per spark.

Here we generalize and apply methods developed for skeletal muscle to determine quantitatively the Ca^{2+} release flux underlying spontaneous Ca^{2+} sparks in cardiac myocytes. The analysis reveals a spatial structure of the flux that is consistent with a multifocal, and probably multichannel origin of the observed sparks.

MATERIALS AND METHODS

$[Ca^{2+}]_i$ was derived from changes in fluorescence, detected using confocal microscopy in single cat atrial myocytes loaded with the Ca^{2+} indicator fluo-3. Atrial myocytes were isolated enzymatically by methods described previously (10). Experiments were performed on freshly isolated cells or on myocytes kept in primary culture for less than 24 h (culture conditions: MEM with 10% fetal bovine serum and 1% penicillin/streptomycin; 5% CO_2; 37°C).

Atrial myocytes were loaded with Ca^{2+} indicator by exposure to 5 μM fluo-3 acetoxymethyl ester (fluo-3/AM; Molecular Probes) for 15 min at 20°C and washing for 20 min in extracellular solution. During the experiments, carried out at 20°C, the cells were continuously superfused with a solution containing 140 mM NaCl, 5 mM KCl, 1 mM $MgCl_2$, 2 mM $CaCl_2$, 10 mM dextrose, and 10 mM Hepes (pH = 7.3, adjusted with NaOH). Fluorescence imaging was performed on a laser scanning confocal microscope (LSM 410; Zeiss) equipped with a ×40 objective (Plan-Neofluar, oil, n.a. = 1.3; Zeiss). Fluo-3 fluorescence was excited with the 488-nm line of an argon ion laser. Emitted light was measured at wavelengths >515 nm. Cellular fluo-3 fluorescence was recorded either in *x–y* (two-dimensional) or line scan mode (512 pixels per line; sampling rate = 250 lines per second). The point spread function was determined with subresolution fluorescent beads, yielding a full width at half amplitude of 0.3 μm in the radial direction. No deblurring procedures were used.

The calculation of $[Ca^{2+}]_i$ as a function of space and time, $[Ca^{2+}]_i(x, t)$, from the fluorescence images, required first the derivation of the total fluo-3 concentration, $dye_T(x)$, which was based on calibrations (developed by Natalia Shirokova, Rush University) as follows. The average field fluorescence intensity was measured in cuvette, at different concentrations of dye and nominal $[Ca^{2+}]$, at many different settings of gain and dark level. At constant $[Ca^{2+}]$, the cuvette calibration data were well fitted by $F = \phi B \exp(b\gamma)\, dye_T + f(\phi, \gamma) + \delta$, where F is fluorescence intensity, ϕ is the applied fraction of the excitation energy, b is a constant, γ is gain, and f is an error term that only becomes significant at high gain (and was offset by δ, the adjustable dark level setting). B, which at high dye concentrations is a slowly

The publication costs of this article were defrayed in part by page charge payment. This article must therefore be hereby marked "*advertisement*" in accordance with 18 U.S.C. §1734 solely to indicate this fact.

0027-8424/97/944176-6$2.00/0
PNAS is available online at **http://www.pnas.org**.

Abbreviations: SR, sarcoplasmic reticulum; $[Ca^{2+}]_i$, intracellular Ca^{2+} concentration.

‡To whom reprint requests should be addressed. e-mail: erios@rpslmc.edu.

decaying exponential function of the vertical position z (as a result of autofiltration), was essentially independent of z at the low dye concentrations used in the experiments. It changed with $[Ca^{2+}]$ as the bracketed expression in Eq. **1** (derived from the expression above neglecting $f + \delta$),

$$F = \phi\left[B_{\min}\frac{K_D + R[Ca^{2+}]}{K_D + [Ca^{2+}]}\right]e^{b\gamma}dye_T. \quad [1]$$

Here K_D is the fluo-3:Ca^{2+} dissociation constant, taken to be 1.0 μM inside the cells (11), B_{min} is the measured value of B at $[Ca^{2+}] = 0$, and R is the ratio of B_{max} to B_{min}, (or of F_{max} to F_{min}, maximum and minimum of fluorescence), equal to 64 in calibrations.

dye_T, a function of position, x, along the scanned line, was calculated replacing F in Eq. **1** by $F_0(x)$, the fluorescence from the line scans averaged over time during the periods of rest before the sparks of interest, and assuming (resting) $[Ca^{2+}]_i$ to be 100 nM. As follows from Eq. **1**, the minimum and maximum fluorescence were derived as $F_{min}(x) = \phi B_{min}\exp(b\gamma)\ dye_T$ and $F_{max}(x) = RF_{min}(x)$.

$[Ca^{2+}]_i(x, t)$ was derived as in ref. 7 in two steps. First the concentration of dye bound to Ca^{2+}, [dye:Ca^{2+}], was derived from the spatially resolved fluorescence $F(x, t)$, using $[dye:Ca^{2+}](x, t) = dye_T(x)\,(F(x, t) - F_{min}(x))/(F_{max}(x) - F_{min}(x))$. Then $[Ca^{2+}]_i(x, t)$ was obtained by solving numerically the equation that describes the evolution of [dye:Ca^{2+}]:

$$\frac{\partial[dye:Ca^{2+}](x,t)}{\partial t} = [dye](x,t)[Ca^{2+}]_i(x,t)k_{ON} - [dye:Ca^{2+}](x,t)k_{OFF} + D_{dyeCa}\Delta[dye:Ca^{2+}](x,t), \quad [2]$$

where [dye] is $dye_T - [dye:Ca^{2+}](x, t)$, D_{dyeCa} is the diffusion coefficient of the complex (0.2×10^{-6} cm^2·s^{-1}; ref. 11), k_{OFF} (70 s^{-1}; ref. 12) and k_{ON} (calculated as 0.7×10^8 M^{-1}·s^{-1}) are the kinetic constants of the dye, and Δ is the Laplacian.

The term spark is used here with three meanings: a localized increase in fluorescence (fluorescence spark), the underlying increase in $[Ca^{2+}]_i$ (Ca^{2+} spark), and the events of release flux that originate it (release spark).

RESULTS

A two-dimensional confocal image of an atrial myocyte is shown in Fig. 1*a*. Fig. 1*b* is a line scan image of fluorescence, obtained by repetitive scanning along the line shown in Fig. 2*a*. The line was positioned parallel to the longitudinal axis of the cell in close proximity to the surface membrane. Thus the observed sparks probably represent Ca^{2+} release from peripheral couplings of the SR (ref. 13; see also ref. 10). Multiple fluorescence sparks are visible in the image. In this cell and in many others, successive sparks appeared to originate from the same spot in the scan. Fig. 1*c* shows in three-dimensional view a line scan image of fluo-3 fluorescence of a spontaneous spark. The increase in fluorescence occupied 2.9 μm at half amplitude, and its amplitude ($\Delta F/F_0 \equiv (F - F_0)/F_0$) was 2.6. From the fluorescence, $[Ca^{2+}]_i(x, t)$ (Fig. 1*d*) was derived as described in *Materials and Methods*.

Deriving Ca^{2+} Release Flux. To understand the channel events underlying a spark, it is necessary to derive the Ca^{2+} flux that determines the increase in concentration. The problem of deriving release flux from $[Ca^{2+}]$ transients has been solved in both skeletal and cardiac muscle, using somewhat different methods. When Ca^{2+} is released, a fraction of it binds to the indicator dye and determines the fluorescence signal, from which the amount and rate of Ca^{2+} binding to the dye can be derived. The rest of the released Ca^{2+} either remains free or is removed by other buffers in the cell. The sole difficulty in "macroscopic" (i.e., cell-averaged) measurements has been to determine this removal rate, which must be added to the rate of change of free and dye-bound Ca^{2+} to calculate release flux. In skeletal muscle, Ca^{2+} removal flux has been derived from the Ca^{2+} transients with the empirical "Melzer" method (14, 15), whereas in cardiac, muscle Sipido and Wier (16) adapted a method developed for skeletal muscle by Baylor *et al.* (17), based on measured properties of the known cellular buffer systems.

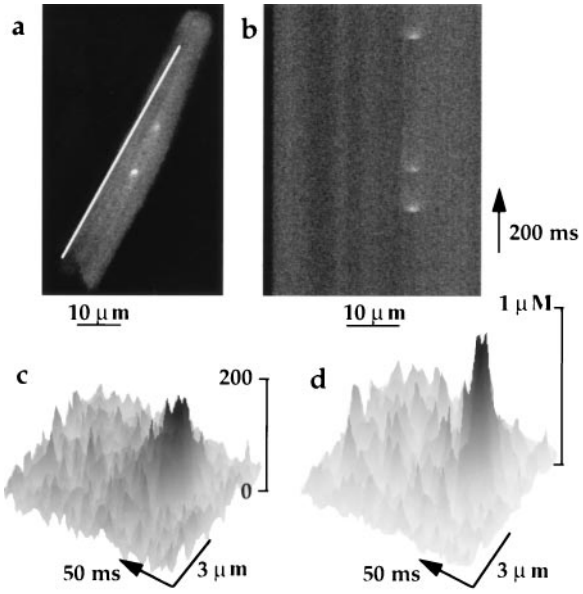

FIG. 1. Repetitive Ca^{2+} sparks in cat atrial myocytes. (*a*) Confocal image (x–y scan; 512 × 512 pixels; pixel size = 0.17 μm) of fluo-3 fluorescence, obtained in a freshly isolated cell. (*b*) Line scan image obtained by repetitive scanning of the subsarcolemmal space every 4 ms along the line in *a*. The line scan image was constructed by stacking 512 lines vertically with time running from bottom to top as indicated by the arrow. (*c*) Three-dimensional representation of a fluorescence spark (fluorescence recorded at 8-bit resolution represented linearly by 256 levels of gray). The resting fluorescence, averaged during the initial 32 ms, varied with position around a value of 48, which was used to derive total dye concentration $dye_T(x)$ ($\simeq$50 μM). The maximum of fluorescence was 180. (*d*) $[Ca^{2+}]_i(x, t)$, derived as described in *Materials and Methods*. Arrows calibrate time as listed.

In this study, we describe a method that combines features of both approaches and generalizes them to derive spatially resolved, heterogeneous Ca^{2+} release flux as a function of space and time.

The basic equation of the Melzer method, which applies to spatially homogeneous changes of $[Ca^{2+}]_i$, is $d\Re/dt = d[Ca^{2+}]/dt + d[Ca^{2+}:dye]/dt + drem/dt$, where $d\Re/dt$ is release flux, $drem/dt$ is removal by cellular buffers and transport systems, and $d[Ca^{2+}:dye]/dt$ is binding by the indicator dye. To derive the spatially heterogeneous release underlying Ca^{2+} sparks, the above-defined functions of time were considered to be also functions of three spatial coordinates. We generalized Melzer's equation as

$$\frac{\partial\Re}{\partial t} = \frac{\partial[Ca^{2+}]}{\partial t} - D_{Ca}\Delta[Ca^{2+}] + (k_{ON,dye}[Ca^{2+}][dye] - k_{OFF,dye}[Ca^{2+}:dye]) + \frac{\partial rem}{\partial t}, \quad [31]$$

which adds a diffusion term, $D_{Ca}\ \Delta[Ca^{2+}]$, where D_{Ca} is the diffusion coefficient and Δ the Laplacian. Additionally, because the Ca^{2+}:dye complex can diffuse, removal of Ca^{2+} by the dye is not $d[Ca^{2+}:dye]/dt$, as in the lumped case, but the term in parentheses in Eq. **3**, which quantifies the net flux of Ca^{2+} into the dye-bound form. In turn, this term can be calculated in terms of the measurable quantity [Ca^{2+}:dye], from the analogous diffusion-reaction equation for the Ca^{2+}:dye species,

$$k_{ON,dye}[Ca^{2+}][dye] - k_{OFF,dye}[Ca^{2+}{:}dye] = \frac{\partial[Ca^{2+}{:}dye]}{\partial t} - D_{Ca:dye}\,\Delta[Ca^{2+}{:}dye]. \quad [4]$$

(A similar qualification applies to the term $\partial rem/\partial t$; it is not the local time derivative of calcium bound to the removal system because this removal system has diffusible components.)

Following Tsugorka *et al.* (7), we approximate $\Delta[Ca^{2+}]$ in Eq. **3** by $3\partial^2[Ca^{2+}]/\partial x^2$. With this approximation, also applied to $\Delta[Ca^{2+}{:}dye]$ in Eq. 4, release flux becomes

$$\frac{\partial \Re}{\partial t} = \frac{\partial[Ca^{2+}]}{\partial t} - 3D_{Ca}\frac{\partial^2[Ca^{2+}]}{\partial x^2} + \frac{\partial[Ca^{2+}{:}dye]}{\partial t} - 3D_{Ca:dye}\frac{\partial^2[Ca^{2+}{:}dye]}{\partial x^2} + \frac{\partial rem}{\partial t}, \quad [5]$$

where every term can be derived from the measured signal, except for the removal flux.

Estimating Removal Flux. Removal flux was calculated as the net rate of binding to saturable compartments, with the kinetic properties of the main Ca^{2+} binding sites of the cardiac cell, namely calmodulin, troponin C, SR binding sites, and phosphocreatine (16), plus transport by the SR pump. The ligands were assumed to be homogeneously distributed in the cytoplasm. The contribution to removal of every mobile ligand was calculated solving a diffusion-reaction equation analogous to Eq. **4**. Removal by the SR Ca^{2+} pump was computed using parameters of Balke *et al.* (18). Because we assumed homogeneously distributed sites and pumping, neither Na/Ca exchange nor sarcolemmal binding sites were included.

The parameters of removal and diffusion are probably different in every cell, and different from published values, measured in different species and conditions. To correct for such errors and the omission of sarcolemmal transport, we used the method of Melzer *et al.* (14, 15), in which the removal parameters are changed until the calculated decay of $[Ca^{2+}]_i(t)$ matches the measured evolution of $[Ca^{2+}]_i(t)$ starting 15 ms after a voltage pulse (a time in excess of that needed for the release channels to close). In the present case, however, we could not apply the method initially on the functions of time because it is not known when the release channels close during a Ca^{2+} spark. Instead, we took advantage of the spatial dimension of the signal and modified removal parameters so that release would be 0 starting at a certain distance from the center of the spark, chosen to be in excess of the presumed radius of the releasing region. The starting distance was 1–2 μm. Extrapolation of the fit then revealed that the radius of the releasing regions was usually 1 μm or less. Among the parameters of removal, we chose to change those of the SR pump. Varying the diffusion coefficients of the Ca^{2+} buffers and assuming, as in previous work (19), a transport rate proportional to the second power of the pump site occupancy, resulted in additional improvements to the fit.

Similar results were found when we used the parameters given by Sipido and Wier (16) for the saturable binding compartments or lumped all contributions in one compartment, similar to the "fast buffer" of Melzer *et al.* (15), of 200 μM concentration, $K_D = 0.4$ μM, $k_{ON} = 10^8\ M^{-1}{\cdot}s^{-1}$, and a diffusion coefficient of 0.3×10^{-6} cm^2/s. This equivalence of a detailed and a lumped model indicates that there is not enough information in the images to fit parameters to the different components of the detailed model, and that the fit should be taken only as a convenient way of parametrizing removal, much in the same way as in the procedure of Melzer *et al.* for skeletal muscle.

Release Flux. Fig. 2 shows the main components in the calculation as they appear in Eq. **5**. $\partial[Ca^{2+}]/\partial t$, which is essentially negligible because most Ca^{2+} is always bound, is not shown. Fig. 2*a* has the Ca^{2+} diffusion term, $-3D_{Ca}\partial^2[Ca^{2+}]/\partial x^2$. The dye

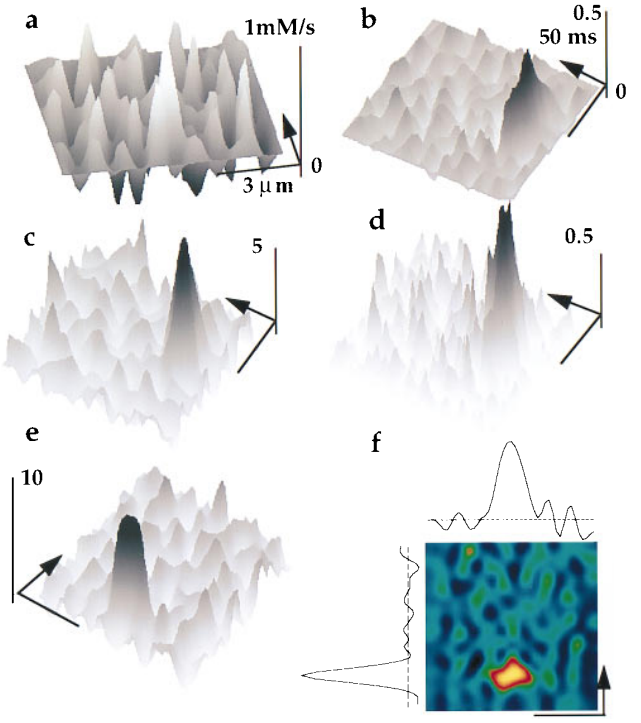

FIG. 2. The components of Ca^{2+} release flux. All terms in Eq. **5** were derived numerically from fluorescence and $[Ca^{2+}]_i$ records in Fig. 1. (*a*) Ca^{2+} diffusion term, $-3D_{Ca}\partial^2[Ca^{2+}]/\partial x^2$, with $D_{Ca} = 3 \times 10^{-6}$ cm$^2{\cdot}$s^{-1} (20, 21). (*b*) Local rate of change of the Ca^{2+}-bound indicator, $\partial[Ca^{2+}{:}dye]/\partial t$. (*c*) Flux of removal by a saturable diffusible buffer of 200 μM concentration, $K_D = 0.4$ μM, $k_{ON} = 10^8\ M^{-1}{\cdot}s^{-1}$, and diffusion coefficient $= 0.3 \times 10^{-6}$ cm^2/s. (*d*) Removal by the pump, with $V_{max} = 1.4$ mM/s, $K_M = 0.3$ μM, and transport rate proportional to the 2nd power of the occupancy (the two terms together constitute $\partial rem/\partial t$ in Eq. **5**.) (*e* and *f*) Two representations of the release flux. In the color plot, blue = 0 and yellow = 10 mM/s. The line plots are averages of release over 40 ms (horizontal plot) or 1.2 μm (vertical) centered at the peak (dashed lines at 0). All time arrows span 50 ms; space calibrations, 3 μm; vertical bars calibrate flux (in mM/s) as indicated.

diffusion term, $3\partial^2[Ca^{2+}{:}dye]/\partial x^2$ (not shown), is similar; both contribute a central peak flanked by negative troughs. In Fig. 2*b* is $\partial[Ca^{2+}{:}dye]/\partial t$, a spatially wide component that becomes negative after the peak of fluorescence. Fig. 2 *c* and *d* represent the removal terms, binding and pump flux, respectively. Finally, Fig. 2 *e* and *f* represent the calculated release flux waveform. As one would expect, the calculated "Ca^{2+} release spark" appears sharper, more restricted spatially and temporally, than the corresponding fluorescence and Ca^{2+} sparks. The line graphs in Fig. 2*f* illustrate that the calculated release was narrow as a function of space and also terminated abruptly as a function of time.

Multifocal Release. In many cells, wider fluorescence sparks were observed; these sparks measured more than 3 and up to 10 μm at half amplitude and were usually greater in amplitude, up to five times the resting fluorescence. The five fluorescence sparks in Fig. 3 *a–e* were obtained in a cell in which we recorded 36 of such wide events, originated from the same site (pixel position 180 ± 1 in the scans). Fig. 3*g* shows the fluorescence averaged over the five sparks (Fig. 3 *a–e*), and Fig. 3*h* plots $[Ca^{2+}](x, t)$, derived from the fluorescence. $[Ca^{2+}](x, t)$ shows an indication of three "lobes" of greater concentration, barely noticeable in the fluorescence average (Fig. 3*f*; see also Fig. 4*e*). Fig. 3 *i* and *j* display the release flux, revealing a triplet of release sparks, separated by distances of about 0.5 μm. As shown in Fig. 3 *k–o*, when the fluorescence events (Fig. 3 *a–e*) were processed individually, the triplet of release sparks was also present, the elementary release sparks then had somewhat different intensi-

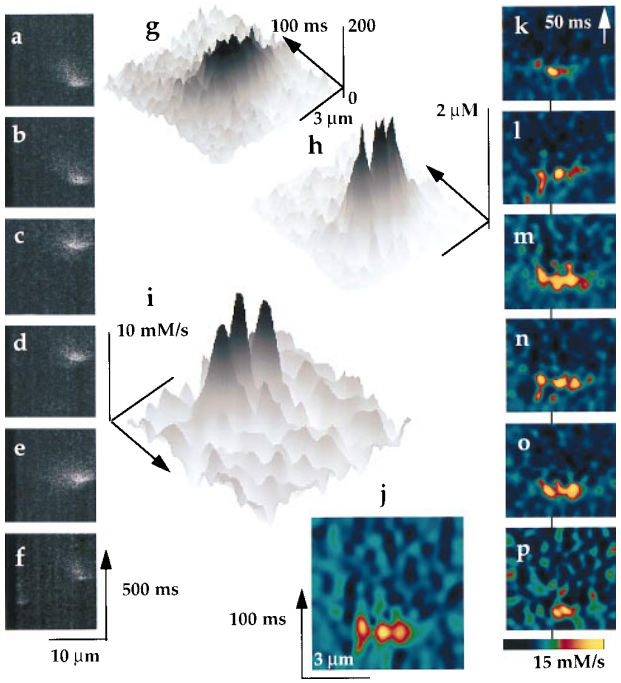

FIG. 3. Multifocal release sparks. (*a–e*) Repeated fluorescence sparks, originated at the same spot in the scan, 13 μm from the edge of the cell. Shown are the first 5 of 36 wide sparks generated in a 10-min interval. (*f*) A narrower spark that originated at the same spot (no. 11 in the sequence). (*g*) Average fluorescence in the five sparks in *a–e*. The average resting fluorescence was 29, the peak 165, and $dye_T(x) \simeq 31$ μM. (*h*) $[Ca^{2+}]_i(x,t)$, derived from the averaged fluorescence. (*i* and *j*) Two representations of the Ca^{2+} release flux, calculated with the parameters given in Fig. 2. (*k–o*) Release flux images derived from the individual fluorescence sparks, showing in all five, indications of three release foci. (*p*) Release from the fluorescence in *f*.

ties and timing but were at the same spatial locations as in the average (the line behind Fig. 3 *j–n* marks pixel position 180 in the original images). Occasionally there were narrower sparks interspersed among the wide sparks (Fig. 3*f*) also centered at pixel 180. In these cases, the calculated flux was missing at least one of the release sparks in the triplet (as shown by Fig. 3*p*, calculated from the narrow spark of Fig. 3*f*).

Several tests were made, on these and other fluorescence images, to rule out an artifactual origin of the release spark multiplets. Fig. 4*a* represents the fluorescence of Fig. 1, Fig. 4*c* is another fluorescence image that gave rise to a doublet of release sparks, and Fig. 4*e* is the average fluorescence of Fig. 3. The images in Fig. 4 *b*, *d*, and *f* were obtained by randomizing the phases in the Fourier transforms shown in Fig. 4 *a*, *c*, and *e*. Therefore, they consist in random noise with the same power spectrum as the corresponding release images. The second row of panels in Fig. 4 represents the results of the release flux calculation algorithm, applied to the corresponding panels in the first row. They show a single release spark for Fig. 4*a*, multiplets of release sparks for Fig. 4 *c* and *e*, and no particular features for the noise images. The third row contains release flux images for the sum of the original fluorescence plus its corresponding noise, showing that the ability of the algorithm to distinguish multiplets was not affected. These tests indicate that the algorithm did not artifactually create the multiple peaks and is robust upon a doubling of noise power.

Another concern was the irregularity in dye distribution, revealed by the inhomogeneous resting fluorescence. The computations of $[Ca^{2+}]$ assume that the dye bound to cell structures behaves like free dye, with the same resting fluorescence and reactivity with Ca^{2+}. The features of the calculated release depend, to some extent, on this assumption. This is illustrated in

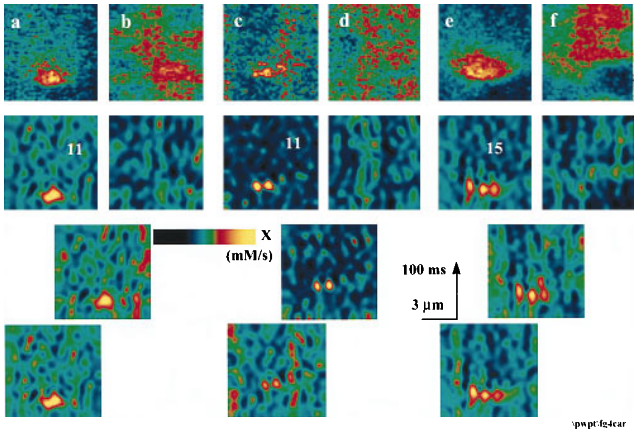

FIG. 4. Tests of the release algorithm. Panels in the first row represent fluorescence data. (*a*) Fluorescence of Fig. 1. (*c*) A fluorescence spark for which the analysis yielded a doublet of release sparks. (*e*) The average fluorescence of Fig. 3*g*. (*b*, *d*, and *f*) Images obtained by randomizing the phases in the Fourier transforms of *a*, *c*, and *e* (the phases were given random values, with adequate symmetry to preserve real inverse transforms; the procedure was repeated four times for each source image; one is shown for each). Second row, release flux calculated from corresponding images in the first row, showing a single release spark for *a*, multiplets for *c* and *e*, and no discernible sparks for the noise images (the numbers in each panel represent the maximum, *X*, in the color table, and apply to release calculated from signal and corresponding noise). Third row, release flux calculated for the sum of the original fluorescence plus its corresponding noise (the two corresponding panels in first row) in the same color scale. Fourth row, release flux from *a*, *c*, and *e*, respectively, assuming that $dye_T(x)$ was constant and equal to its average.

the fourth row of Fig. 4, in which we recalculated the flux for the three fluorescence images (Fig. 4 *a*, *c*, and *e*) assuming a constant concentration of reactive dye (or equivalently, that only the free dye was capable of reacting). The assumption did not cause qualitative changes, except for Fig. 4*c*, in which a region of steady elevation of fluorescence was interpreted as due to an almost steady release. Other parameters of the dye were changed in tests, including diffusion coefficient (by a factor of 5) and kinetic constants (by a factor of 2), without significant qualitative consequences; multiplicity remained in all images analyzed with different assumptions and parameter values.

Whether release sparks were single or multiple did not depend on removal parameters. For example, when the fluorescence spark in Fig. 3*g* was fitted with a different set of parameter values, including a fast buffer compartment of two times greater concentration, the peak value of release flux increased 50%, but the triplet structure was not affected. Therefore, and as was the case in skeletal muscle (19), the determination of kinetic and spatial properties of release was robust; it did not depend steeply on the parameters of removal, provided that the fit of the transients was good.

Finally, the fact that narrow and wide fluorescence sparks were observed at the same location indicates that the wide, multifocal feature of these fluorescence signals was not due to local structural restrictions to diffusion.

Multifocal release sparks were found repeatedly, in many cells. Most of them were derived from fluorescence sparks of more than 3 μm, which already featured spatial heterogeneity and constituted roughly 20% of all sparks examined. Doublets and triplets had variable spatial separation, suggesting that the spatial distance between discrete release sparks is variable in different regions. When the separation was large, the events tended to be separated in time, by intervals consistent with a finite propagation speed of about 60 μm/s (Fig. 5). Fig. 5 also illustrates that the fluorescence increases in those cases were very large in amplitude (4.8 times the resting fluorescence in Fig. 5*b*).

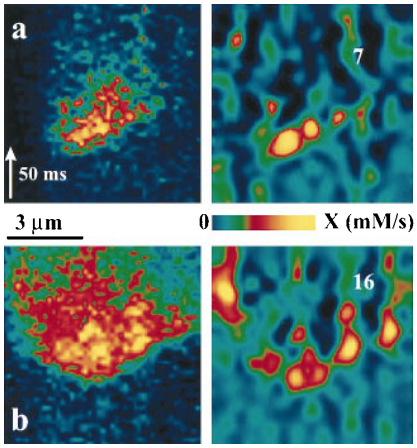

FIG. 5. Propagating release. (*Left*) Fluorescence. (*a*) $F_0(x) \simeq 40$; $dye_T(x) \simeq 42$ μM; maximum fluorescence = 163. (*b*) $F_0(x) \simeq 43$; $dye_T(x) \simeq 45$ μM; maximum fluorescence = 248. (*Right*) Release flux, calculated with the same parameters as in previous figures (numbers represent the maximum in the color scale).

Eight fluorescence sparks narrower than 3 μm at half amplitude, and 36 of 3 μm or more were analyzed with this algorithm. All narrow fluorescence sparks gave single release sparks, with average amplitude = 7.1 ± 1.4 mM/s, full width at half maximum (fwhm) 1.6 ± 0.2 μm, and duration at half amplitude = 22 ± 4 ms. Twenty of the wide sparks analyzed gave well defined multiplets of release sparks. Among the individual peaks within multiplets, 41 had amplitude greater than 3.3 mM/s (the average minus two SEMs of the singlets), averaging 8.1 ± 0.4 mM/s. Their duration at half amplitude was 23 ± 4 ms, and the fwhm (measured on one side of the sparks in multiplets) was 1.2 ± 0.2 μm. None of the average measures were statistically different in singlet release sparks and sparks in multiplets. Individual peaks of up to 16 mM/s were observed.

DISCUSSION

Ca^{2+} sparks, which in cardiac myocytes occur spontaneously or in response to activation of L-type Ca^{2+} currents, are generally viewed as the result of Ca^{2+} release from functional units of the SR. Since the Ca^{2+} sparks evoked by L-type Ca^{2+} current are relatively uniform, independent of voltage, and occur in close vicinity to the transverse tubular membrane in ventricular myocytes, it is believed that Ca^{2+} sparks represent the elementary event underlying excitation–contraction coupling in the heart (2, 3, 4, 9, 22, 23, 24). Whether a Ca^{2+} spark results from the opening of a single ryanodine receptor or a number of channels acting in concert is still debated (25).

To address this issue, we derived Ca^{2+} release flux from local Ca^{2+} signals in quiescent cardiac myocytes, extending the methods developed for skeletal muscle by Baylor *et al.* (17) and Melzer *et al.* (14, 15). As was the case in the previous studies in both skeletal and cardiac muscle, the main obstacle was the determination of Ca^{2+} removal flux (by binding and SR pumping). In the present case, we used Ca^{2+} binding parameters estimated for guinea pig ventricular myocytes (16) and then adjusted other parameters to fit the Ca^{2+} transients, as done in skeletal muscle (14, 15, 19). In skeletal muscle, the process of adjustment of parameters assumes that release stops a few milliseconds after the end of a depolarizing voltage clamp pulse. In the present case of spontaneous Ca^{2+} spark activity, in which $[Ca^{2+}]$ is a function of time and space, we first used the spatial dimension of the signal to modify the fitting parameters, assuming that release was restricted to the immediate vicinity (1-μm radius) of the center of the Ca^{2+} spark. A good fit of removal resulted in release waveforms like the ones shown, in which release appears to originate in regions about 1 μm wide, single in the majority of cases but multiple in many cases.

The present algorithm yields release flux, in intensive units of millimolar per second, as the change in total $[Ca^{2+}]$ determined in the associated cytoplasm in 1 s. The flux in moles per second was obtained integrating the intensive flux over the associated volume. We did this assuming a radially symmetrical distribution of release in the focal plane (x, y), proportional to $\exp(-(x^2 + y^2)/2\sigma)$ and constant over the z dimension of the confocal resel, assumed to be 1 μm high. For example, a spark of release with average dimensions, peak release flux of 7 mM/s, and width at half amplitude of 1.5 μm (or $\sigma = 0.64$ μm), would have an integrated flux of 1.5×10^{-17} mol/s, or 3 pA.

The value 3 pA is two times the current estimated by Tinker *et al.* (26) for a single cardiac release channel *in vivo* (based on bilayer measurements extrapolated to intracellular conditions using an Eyring rate model of permeation and an intra-SR $[Ca^{2+}]$ of 1.5 mM; ref. 27). On this basis alone, the present results would indicate that sparks of release could arise at single channels. A more careful consideration of the present results, in light of previous work on skeletal muscle, favors instead a multichannel origin.

A first argument is made based on the evidence (25) that sparks originate at junctions of known geometry. In cardiac cells, Ca^{2+} release is controlled at couplings between the SR and either the sarcolemma or transverse tubuli, termed peripheral couplings and dyads or triads, which in cat atria (13) are roughly circular, with a diameter of 0.2–0.6 μm. These dimensions are consistent with the size of the regions where the individual release sparks originate, when allowance is made for the additional spread introduced by the imaging optics. Assume that J_0 moles per second of an ion of diffusion coefficient D are injected at the center of a volume shaped like the cleft in a peripheral junction, a cylinder of radius R and height ε, from which the injected ion can only exit at the edge (the cylindric surface). A steady state will be rapidly reached (28), in which the flux that is injected exits at the edge, and a profile of concentrations is established, decaying from a maximum at the center to a minimum at the edge. We derived the relationship $C(R) = J_0/[2\pi D(2\varepsilon R)^{1/2}]$ for the concentration at the edge of the cleft (approximating the problem to that of unrestricted flow from a sphere of the same area as the cylindric surface). Using $J_0 = 1.5 \times 10^{-17}$ mol/s, or 3 pA, $D = 3 \times 10^{-6}$ $cm^2 \cdot s^{-1}$, $r = 250$ nm, and $\varepsilon = 15$ nm, $C(R)$ is 45 μM. M. Stern (National Institute of Aging, Baltimore) computed the numerical solution of the cylindric diffusion problem and found $C(R) = 78.3$ μM. Since this is the minimum concentration that other channels will face inside the junction, and it is reached very rapidly, every release channel in the junction should be activated. Similarly, Langer and Peskoff (29) calculated that a 20-ms release of Ca^{2+} from junctional SR during normal excitation–contraction coupling elevates $[Ca^{2+}]$ to 600 μM at the center and 100 μM at the periphery in the diadic cleft. Multiple channels should be present in a typical coupling, forming arrays with interchannel distances of 30 nm (30). Currents of the size estimated here for a single spark, if injected into a junctional gap, should result in rapid increases of $[Ca^{2+}]$ to levels well beyond those that activate release channels in bilayers. Just the magnitude of the calculated release flux, therefore, makes it unlikely that release channels within a junction activate independently.

Other arguments stem from the observation of release spark multiplets. Multiplets of release sparks span distances of up to 7 μm (Fig. 5*b*), and more in images not shown. Therefore, all sparks within a multiplet could not have originated from the same junction. In chicken ventricle, which shows ultrastructural similarities with mammalian atrial muscle (13, 30), Protasi and Franzini-Armstrong (31) measured an average distance of approximately 0.5 μm between peripheral junctions. This distance is similar to the separation between adjacent sparks within multiplets, which suggests that the release multiplets originated from multiple junctions.

Given the low frequency of sparks in general, release sparks in multiplets cannot have occurred together just by random temporal coincidence. One of the sparks must have caused the others. This implies that release activation can propagate, jumping across hundreds of nanometers, from one junction to another [a conclusion reached previously on different grounds by Sommer *et al.* (32) and Protasi and Franzini-Armstrong (31)]. This conclusion is also similar to one reached for rat ventricular muscle (9) on the basis of transversal scanning within a Z disk, which suggests that the propagation of sparks within short distances is not limited to cat atrial cells. Propagation between junctions also must be involved in the generation of "macrosparks," Ca^{2+} sparks of large amplitude and wider spatial spread that can form the site of origin of calcium waves (2).

That the activation of release can propagate between junctions strengthens the conclusion reached before: the opening of one channel within a junction should result in the activation of the other channels in the same junction. The alternative, that the activation propagates hundreds of nanometers between junctions but not tens of nanometers within junctions, seems untenable.

This argument, however, depends on the assumption that sparks originate at junctions. Could they have originated outside junctions, at individually activating, isolated channels? The magnitude of the sparks, and their associated release current, make this possibility unlikely. The maximum of $\Delta F/F_0$ in fluorescence sparks shown here was between 1 and 4.8, whereas in skeletal muscle, it was about 0.8 for selected sparks (33), or 0.3 for the elementary event amplitude detected by Tsugorka *et al.* (7). In agreement with the difference in magnitude of the fluorescence events, the release flux estimated here is greater than the estimate for individual events of skeletal muscle (N. Shirokova and E.R., unpublished work). Considering that in bilayers currents are somewhat smaller for cardiac than for skeletal muscle channels (34), then the individual release sparks of cardiac muscle should involve more channels than in skeletal muscle. This indicates that more than one channel should be involved in a cardiac Ca^{2+} spark.

The strikingly different structural patterns of molecular arrangement in excitation–contraction coupling junctions of skeletal and cardiac muscle may result in different rules for association of channels to generate the elementary events of release. Although the pattern in cardiac muscle is two-dimensional (release channels arranged regularly in a planar, roughly circular specialized membrane), in skeletal muscle, it is one-dimensional (a double row of release channels). These different geometric patterns are accompanied by very different local restrictions for diffusion, which should make the concentration gradients associated with channel opening more localized in skeletal muscle. The differences in structure and in sensitivity of the release channels to activation by Ca^{2+} (34), together with the observed differences in the release sparks, suggest that the control of skeletal muscle release channels is more detailed, probably involving activation by calcium, but restricted to a domain of tens of nanometers, a "nanodomain," containing one or a few channels (12). In cardiac muscle instead, many more release channels should respond together in the "microdomain" of the junction.

We thank Christine E. Rechenmacher for her expert technical assistance, Dr. Natalia Shirokova (Rush University) for calibrating the relationship between fluorescence and dye concentration, Dr. M. Stern (National Institute of Aging, Baltimore) for the numerical solution of the cylindrical diffusion problem, Dr. D. Chen (Rush University) for help with the approximate analytical solution, and Drs. D. G. Ferguson (University of Cincinnati, Cincinnati) and C. Franzini-Armstrong (University of Pennsylvania, Philadelphia) for discussions on muscle structure. The cells were kindly provided by Dr. S. L. Lipsius (Department of Physiology, Loyola University Chicago). Financial support was obtained from National Institutes of Health Grants HL51941 (to L.A.B.) and AR32808 (to E.R.), the American Heart Association National Center (L.A.B. and E.R.), the Muscular Dystrophy Association (E.R.), and the Schweppe Foundation Chicago (L.A.B.). L.A.B. is an Established Investigator of the American Heart Association. J.H. is a postdoctoral fellow of the Deutsche Forschungsgemeinschaft.

1. Fabiato, A. (1983) *Am. J. Physiol.* **245,** C1–C14.
2. Cheng, H., Lederer, W. J. & Cannell, M. B. (1993) *Science* **262,** 740–744.
3. López-López, J. R., Shacklock, P. S., Balke, C. W. & Wier, W. G. (1994) *J. Physiol. (London)* **480,** 21–29.
4. López-López, J. R., Shacklock, P. S., Balke, C. W. & Wier, W. G. (1995) *Science* **268,** 1042–1045.
5. Cheng, H., Cannell, M. B. & Lederer, W. J. (1995) *Circ. Res.* **76,** 236–241.
6. Xiao, R.-P., Lakatta, E. G. & Cheng, H. (1996) *Biophys. J.* **70,** A245.
7. Tsugorka, A., Ríos, E. & Blatter, L. A. (1995) *Science* **269,** 1723–1726.
8. Lipp, P. & Niggli, E. (1996) *J. Physiol. (London)* **492,** 31–38.
9. Parker, I., Zang, W.-J. & Wier, W. G. (1996) *J. Physiol. (London)* **497,** 31–38.
10. Hüser, J., Lipsius, S. L. & Blatter, L. A. (1996) *J. Physiol.* **494,** 641–651.
11. Harkins, A. B., Kurebayashi, N. & Baylor, S. M. (1993) *Biophys. J.* **65,** 865–881.
12. Ríos, E. & Stern, M. D. (1997) *Annu. Rev. Biophys. Biomol. Struct.* **26,** 47–82.
13. McNutt, N. S. & Fawcett, D. W. (1969) *J. Cell Biol.* **42,** 46–67.
14. Melzer, W., Ríos, E. & Schneider, M. F. (1984) *Biophys. J.* **45,** 637–641.
15. Melzer, W., Ríos, E. & Schneider, M. F. (1987) *Biophys. J.* **51,** 849–864.
16. Sipido, K. R. & Wier, W. G. (1991) *J. Physiol. (London)* **435,** 605–630.
17. Baylor, S. M., Chandler, W. K. & Marshall, M. W. (1983) *J. Physiol. (London)* **344,** 625–666.
18. Balke, C. W., Egan, T. M. & Wier, W. G. (1994) *J. Physiol. (London)* **474,** 447–462.
19. González, A. & Ríos, E. (1993) *J. Gen. Physiol.* **102,** 373–421.
20. Ríos, E. (1994) in *Bioelectrochemistry IV: Nerve Muscle Function*, eds. Melandri, B. A., Milazzo, G. & Blank, M. (Plenum, New York), pp. 9–29.
21. Kushmerick, M. J. & Podolsky, R. J. (1969) *Science* **166,** 1297–1298.
22. Cannell, M. B., Cheng, H. & Lederer, W. J. (1994) *Biophys. J.* **67,** 1942–1956.
23. Cannell, M. B, Cheng, H. & Lederer, W. J. (1995) *Science* **268,** 1045–1049.
24. Shacklock, P. S., Wier, W. G. & Balke, W. (1995) *J. Physiol. (London)* **487,** 601–608.
25. Cheng, H., Lederer, M. R., Xiao, R.-P., Gómez, A. M., Zhou, Y.-Y., Ziman, B., Spurgeon, H., Lakatta, E. G. & Lederer, W. J. (1996) *Cell Calcium* **20,** 129–140.
26. Tinker, A., Lindsay, R. G. & Williams, A. J. (1993) *Cardiovasc. Res.* **27,** 1820–1825.
27. Chen, W., Steenbergen, C., Levy, L. A., Vance, J. London, R. E. & Murphy, E. (1996) *J. Biol. Chem.* **271,** 7398–7403.
28. Stern, M. D. (1992) *Biophys. J.* **63,** 497–517.
29. Langer, G. A. & Peskoff, A. (1996) *Biophys. J.* **70,** 1169–1182.
30. Sun, X.-H., Protasi, F., Takahashi, M., Takeshima, H., Ferguson, D. G. & Franzini-Armstrong, C. (1995) *J. Cell Biol.* **129,** 659–671.
31. Protasi, F. & Franzini-Armstrong, C. (1996) *Biophys. J.* **70,** A245.
32. Sommer, J. R., Bossen, E., Dalen, H., Dolber, P., High, T., Jewett, P., Johnson, E. A., Junker, J., Leonard, S., Massar, R., Scherer, B., Spach, M., Spray, T., Taylor, I., Wallace, N. R. & Waugh, R. (1991) *Acta Physiol. Scand.* **142,** Suppl. 599, 5–21.
33. Klein, M. G., Cheng, H., Santana, L. F., Jiang, Y.-H., Lederer, W. J. & Schneider, M. F. (1996) *Nature (London)* **379,** 455–458.
34. Meissner, G. (1994) *Annu. Rev. Physiol.* **76,** 485–508.